CHAPTER 4

STRENGTH PROPERTIES OF HYDROXYAPATITE CERAMICS

Having provided the background theory of indentation fracture mechanics, together with the possible toughening mechanisms and mechanics of grain-localized bridging at the crack interface behind the advancing crack tip and phase transforming of zirconia from tetragonal to monoclinic under the influence of the applied stress (Chap.3), we are now in a position to investigate fracture properties of our prepared HAp specimens (Chap.2), using the indentation-technique.

4.1 The Response of HAp ceramics to Vickers Indentations

In this section, we will examine the response of HAp specimens to the Vickers indentation. Although the indentation cracks are artificially introduced entities, there is a considerable evidence that they do indeed simulate the essential qualities of naturaliy occurring surface flaws in ceramic components (30). Therefore this examination will reflect the mechanics of formation of naturally occurring surface cracks which have contact history (Sect.3.3).

4.1.1 Experimental Procedure

In order to be able to observe its deformation/fracture patterns proceduced by the Vickers indentation, the preexisting damages on specimen surfaces have to be removed by polishing with sucessively finer abrasive powders to obtain an optical finish. In this wotk, the optimum surface-removing procedure was achieved by polishing the specimen surface with a series of SiC paper (800,1200 mesh), and a series of alumina powders in water slurry (1, 0.5, 0.03 μm). When the polishing process was completed, the specimen was indented by a Vickers indenter at various indentation loads using a hardness testing machine (Zwick). Loading of the indenter was under dead-weight conditions with rates controlled by an adjustable dashpot (loading velocity 1 mm s^{-1}), unloading was by hand and was somewhat more rapid. The peak contact load was maintained for 10-15 s. During indentation, care was

taken to maintain the indentation axis parallel to the surface normal of specimen and indents spaced far enough apart that no measurable crack interactions occurred. Specimen surfaces, the indenters and the indenter stage were well cleaned with solvents prior to indenting. All indentations were made in ambient air. The contact site was positioned at the specimen center. After each indentation, the deformation/fracture pattern of the indented specimen was exmined by an optical microscope operated in reflected light and/or a scanning electron microscope. Measurements of the dimensions of crack, c , and impressional half-diagonal, a, were made with the optical microscope.

To enable an investigation of the fracture mode* in our HAp specimens, some indented specimens were subjected, some indented specimens were subjected to a thermal etching at a temperature 10°C below the sintering temperature (i.e.1190°C) for 10 min to reveal their grain structures. These thermal etched surfaces were then coated with thin gold layers before being examined for the fracture mode by a scanning electron microscope.

4.1.2 Results

The response of HAp specimens to the Vickers indentation will be presented in two parts : the first is a qualitative description of the deformation and fracture behavior, and the second presents quantitative results.

4.1.2.1 Qualitative Description

The main observations of the influence of indentation load on the HAp surface are the followings :

(i) Cracking occurs even for the load as low as 1 N. Fig. 4.1 shows the observed damage pattern due to 1 N-load.

---

* The fracture mode is said to be intragranular if the crack path passes through grains and it is termed intergranular if the crack path is along grain boundaries.

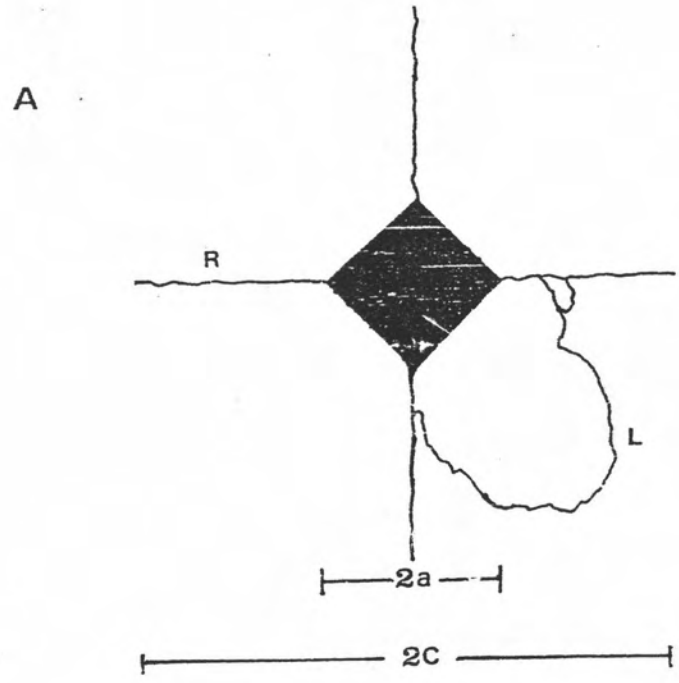

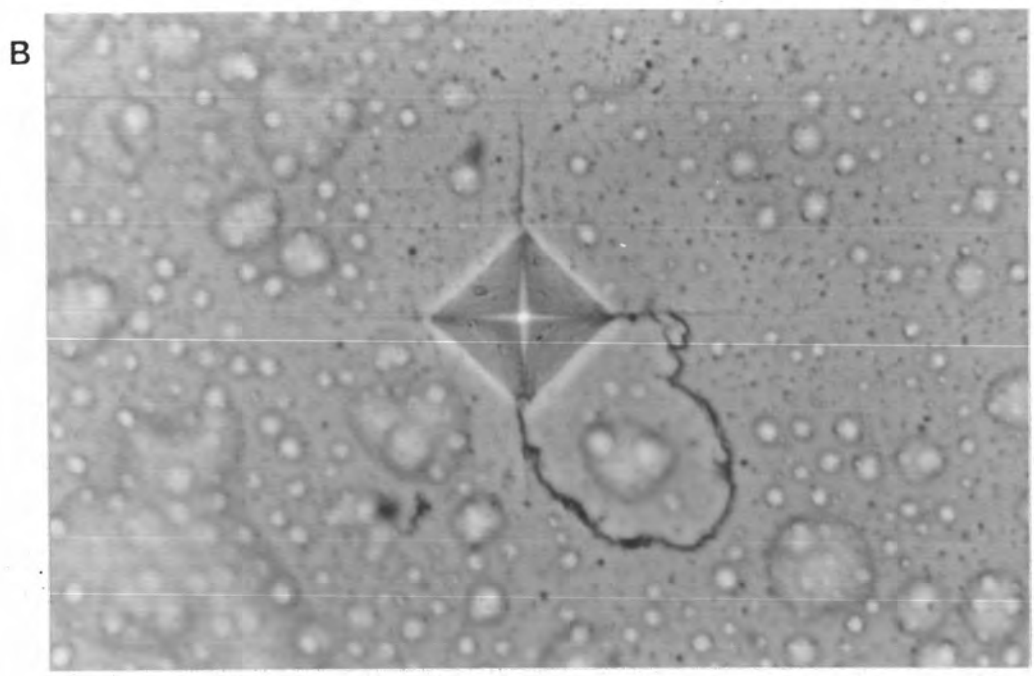

Fig.4.1 Schematic and optical micrograph (X 1000) of Vickers-produced damage pattern on surface of HAp specimen indented with 1 N load.
(A) schematic diagram. Also label in (A) is radial (R) crack, lateral (L) crack and residual impression (shaded), (B) optical micrograph.

(ii) Cracks are of two types : median/radial and lateral. The median/radial cracks form on the two mutually orthogonal median planes of symmetry defined in each case by the indentation axis and one of the impression diagonals, centered on the indentation point and is axis and one of the impression diagonals, centered on the indentation point and is residual impression (shaded) (Fig.4.1).

The lateral cracks form nearly parallel to the specimen surface and center beneath the contact zone. The deflection of the lateral crack towards the specimen surface is evident in Fig. 4.1 as surface trace (L) on the bottom right quarter of the damage pattern.

(iii) The higher the indentation load, the more severe the damage pattern. Fig. 4.2 shows the observed damage pattern due to 5 N load in comparison with that due to 10 N load. Apart from the longer radial traces due to the 10 N load, the more severe chipping due to lateral cracks intersecting the specimen surface is evident in Fig.4.2. Fig.4.3 shows the SEM micrograph of damage pattern due to 20 N load. It is noted that for the indentation loads $\geq$ 20 N the residual impression corners on specimen surface is no longer well defined, (Fig.4.3b). For the indentation loads above 30 N, the lateral cracks produce so intense surface chipping that the crack patterns are no longer seen.

(iv) The fracture in the HAp specimen is intragranular. Fig 4.4 shows that the indentation crack path in the HAp specimen passes through the grains.

4.1.2.2 Quantitative Results

4.1.2.2.1 Indentation Load Dependence of Impression Half-Diagonal of HAp Specimen

Having pointed out in the previous section (Sect.4.1.2.1) that the corner of residual impression due to the indentation loads $\geq$ 20 N were not well-defined, therefore only tests performed in the 1 to 15 N load range were retained for hardness measurements. Fig.4.5 represents the impression half-diagonal, a, (Fig.4.1 a) as a function of the indentation load. The dimension of impression half-diagonal for each indent was measured as averages over the two half-diagonals. Each data point in Fig. 4.5 represents the mean and stardard deviation of

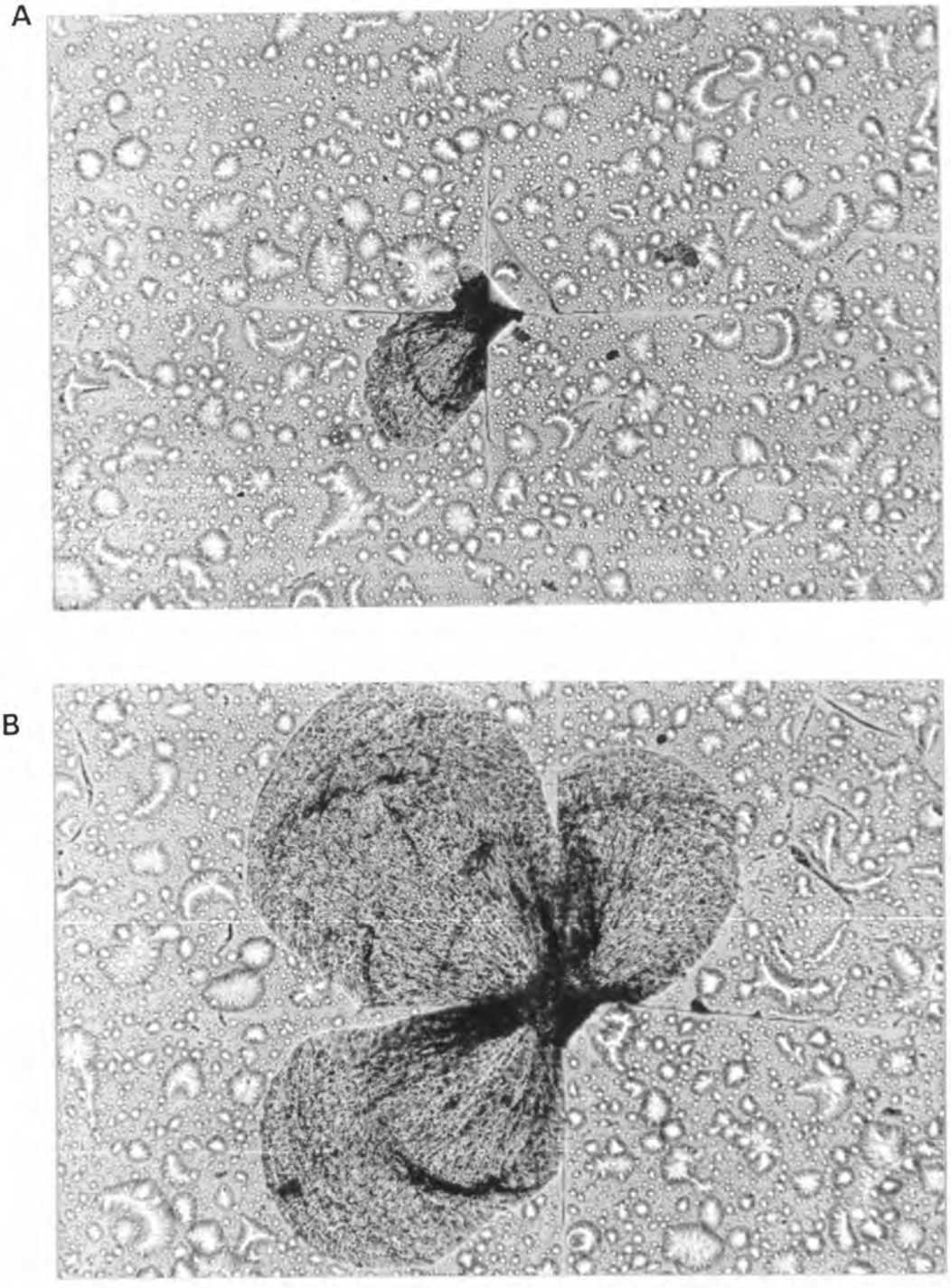

Fig.4.2 Optical micrograph (X 200) of Vickers-produced damage patterns on surface of HAp specimen indented at two different loads.
(A) indentation load = 5 N, (B) indentation load = 10 N.

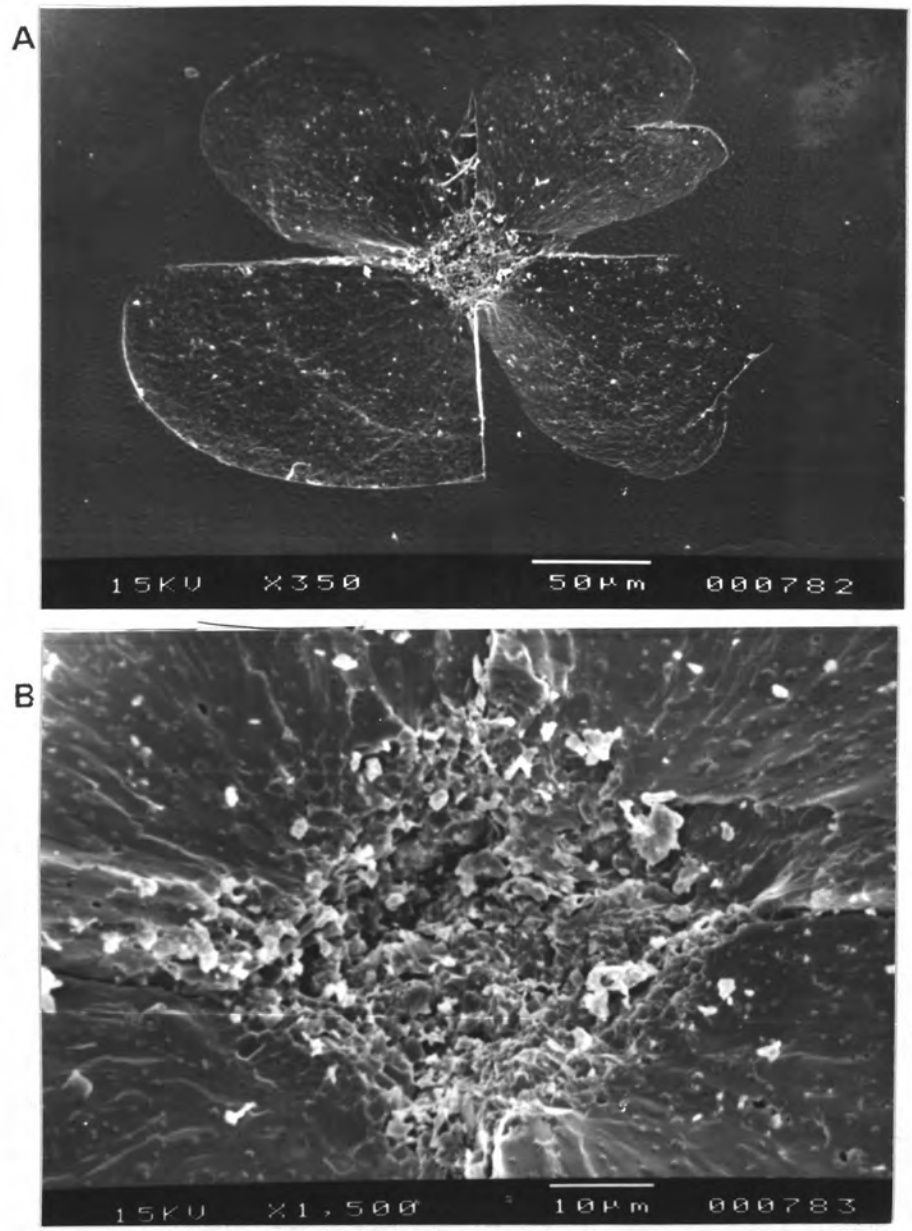

Fig.4.3 SEM micrograph of Vickers-produced damage patterns on surface of HAp specimen indented with 20 N load.

(A) whole damage pattern, (B) area around residual impression.

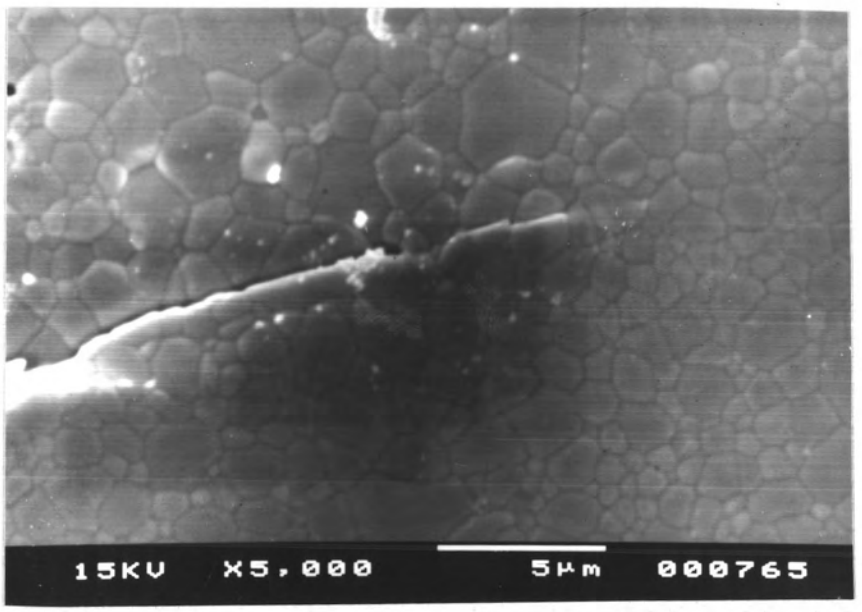

Fig.4.4 SEM micrograph of an indentation crack path on surface of HAp specimen.

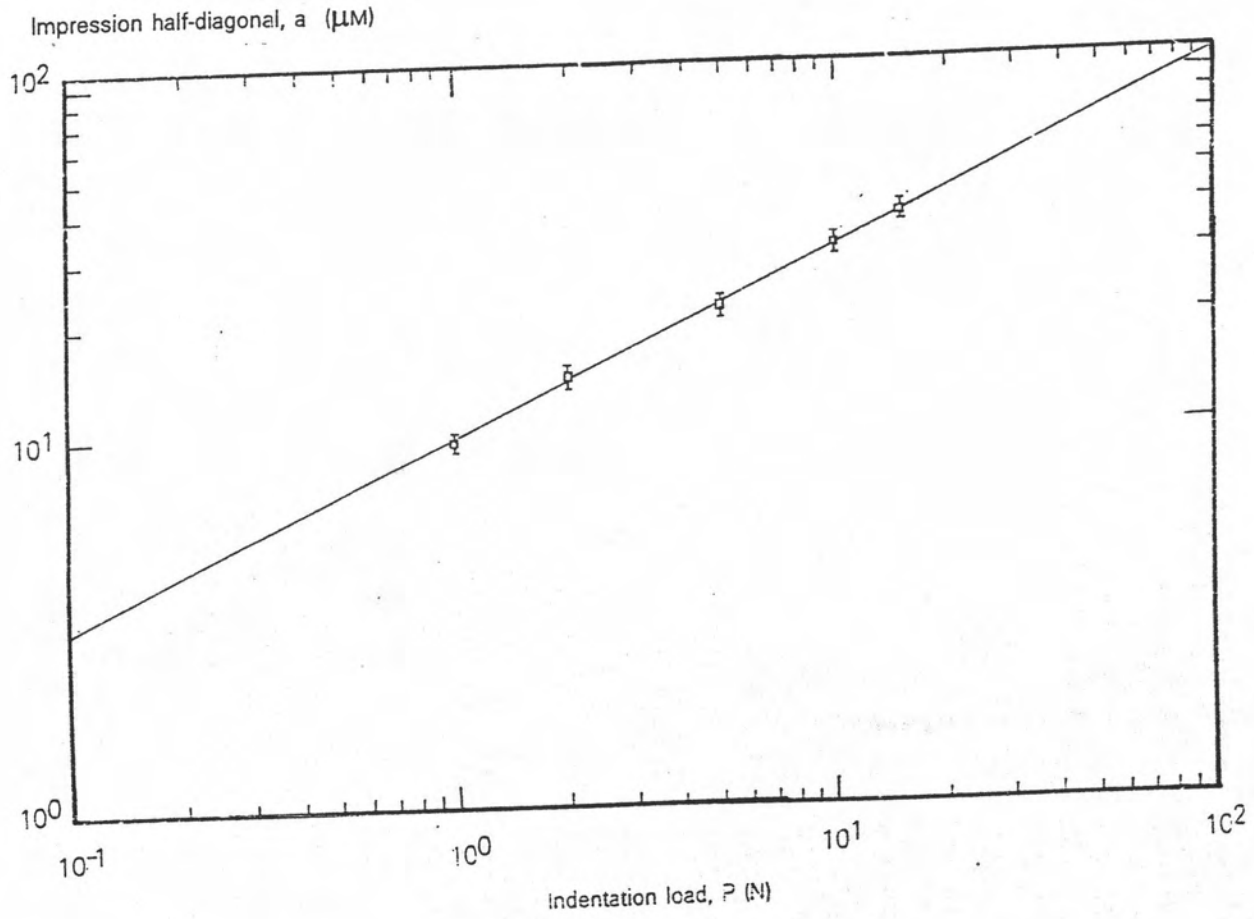

Fig.4.5 Plot of impression half-diagonal, a, as a function of indentation load, P.

five indentations. The result illustrated in Fig. 4.5 has established that the dimension of impression half-diagonal in HAp follows the 1 / 2 power dependence of indentation load (a α $P^{1/2}$). Thus the above obtained dependence of a on P implies that Eq. (3.18) is the equation to be used for evaluating hardness H for the HAp specimens. Fig.4.6 resummarizes the results of impression half-diagonal measurements as a plot of P/a^2 as a function of indentation load P and the fitted line is the mean over all indentations. It can be seen from such plot that the mean value of P/a^2 = 10.6 $\pm$ 0.8 GPa. From Eq.(3.18) along with the mean value of P/a^2, we obtain H = 5.3 $\pm$ 0.4 GPa for HAp specimens.

4.1.2.2.2 Indentation Load Dependence of Radial Crack Length of HAp Specimen

In the same manner as above, the radial crack length was studied as a function of indentation load. Again due to difficulties in accurately measuring radial crack length when $P \geq$ 30 N. Tests performed in the 2 to 20 N load range were retained for the radial crack length measurement. The indentation load dependence of the radial crack length c, is presented in Fig. 4.7. Each radial cracklength was measured as average over the four radial traces. Each data point in Fig.4.7 represents the mean and standard deviation of five indentations. The slope of c-P curve in Fig.4.7 is 2/3. Thus the results illustrates in Fig.4.7 has established that the dimension of the radial crack in HAp specimens follows the Eq.(3.22) (c α $P^{2/3}$). Fig.4.8 resummarizes the result of crack measurements as a plot of $P/c^{3/2}$ as a function of indentation load P and the fitted line is the mean over all indentations. The mean value of $P/c^{3/2}$ = 8.1 $\pm$ 0.1 $MPa^{1/2}$.

4.2 Evaluation of Fracture Toughness of HAp Specimen

The fracture toughness, T, can be evaluated from the value of $P/c^{3/2}$, using Eq.(3.22). However the ratio E/H is required in the determination. In this work we will use a simple indentation technique developed by Marshall et al. (52) for measuring the hardness-elastic-modulus ratio, H/E. The method is based on a measurement of the elastic recovery of the in-

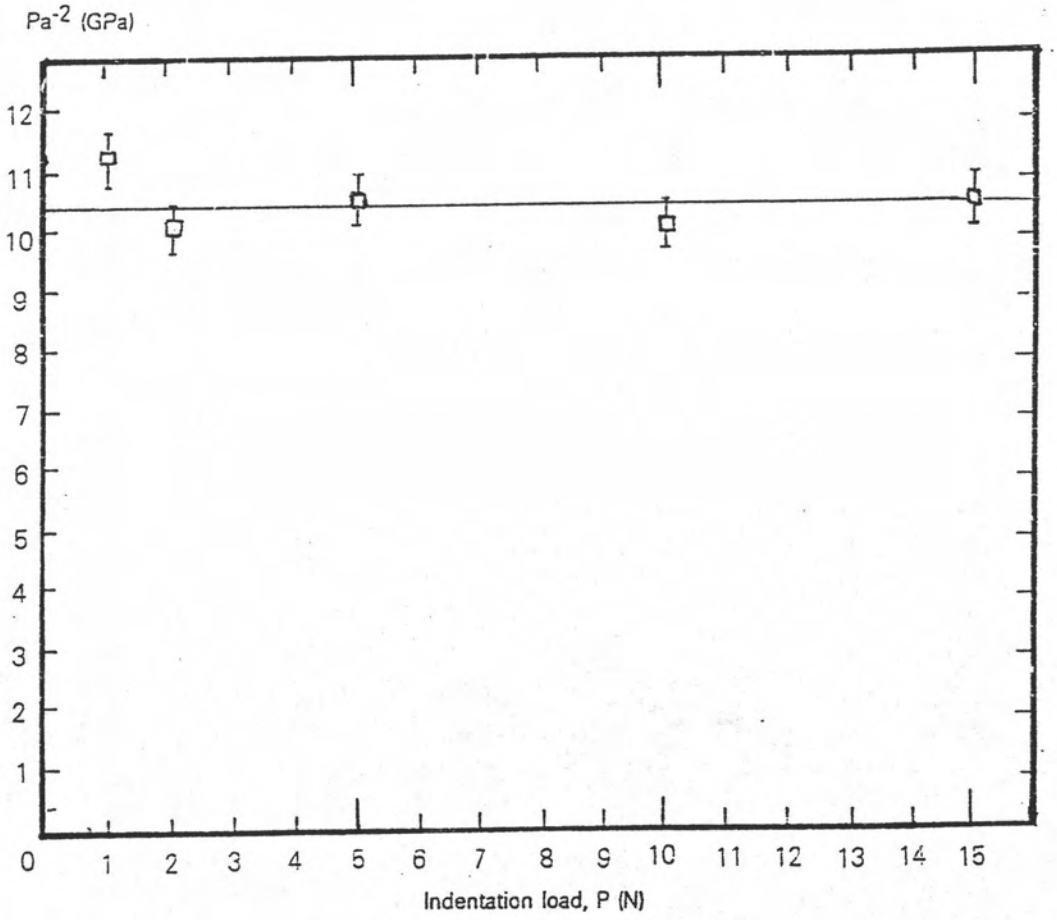

Fig.4.6 Plot of P/a^2 as a function of indentation load, P.

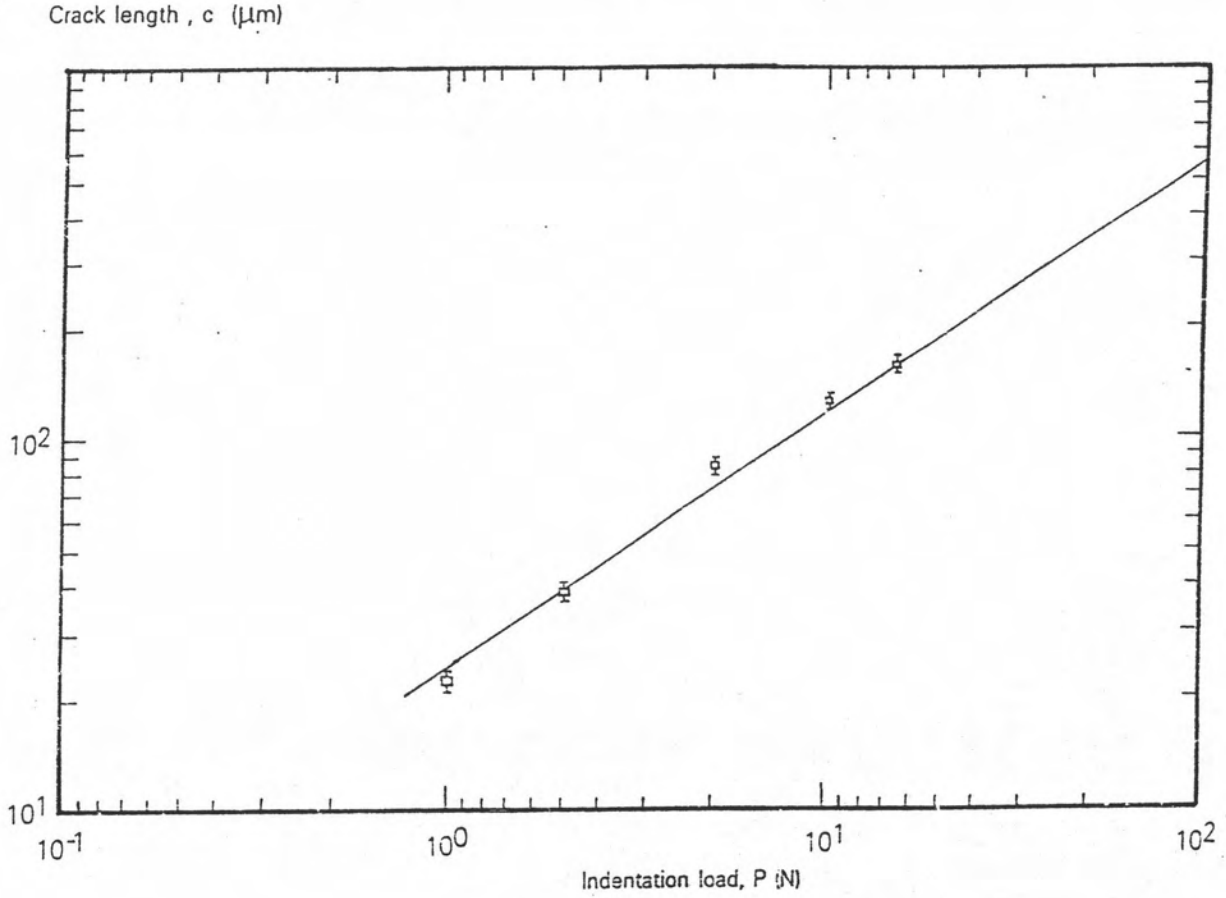

Fig.4.7 Plot of radial crack length, c, as a function of indentaion load, P.

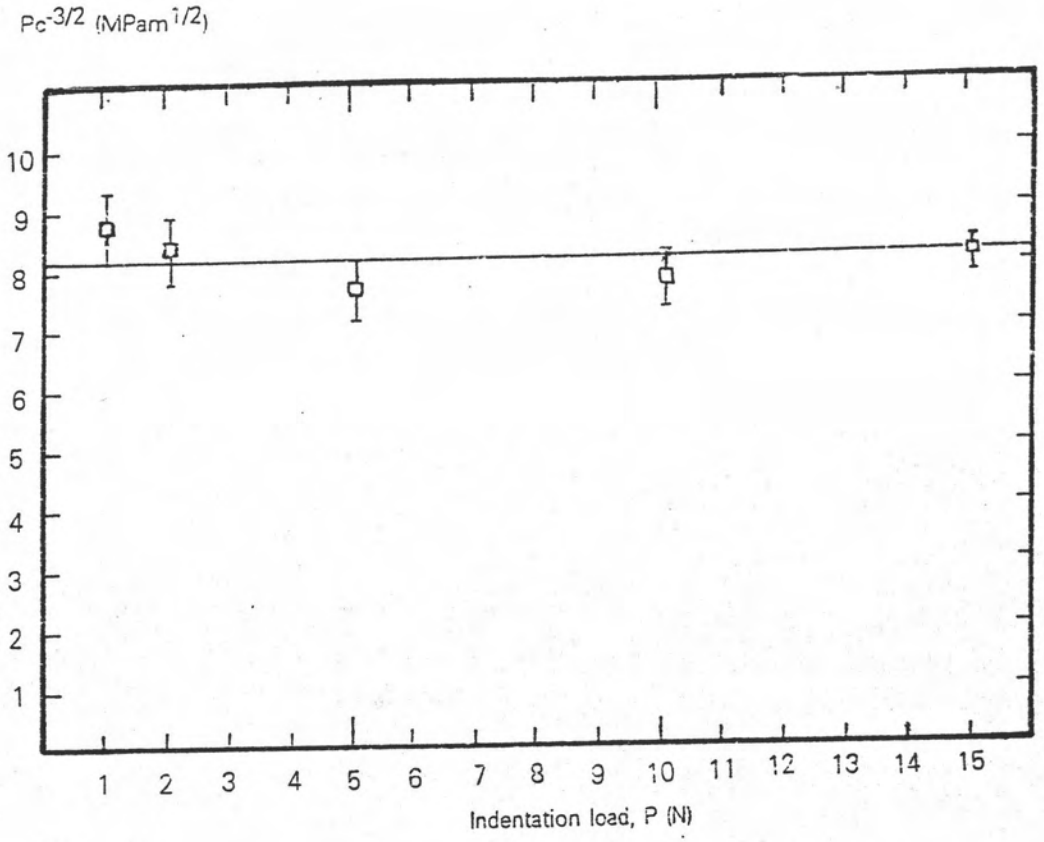

Fig.4.8 Plot of $P/c^{3/2}$ as a function of indentation load, P.

surface dimensions of a Knoop diamond indentation, as show in Fig.4.9. Under a load P, the ratio of the diagonal dimension, a and b, at the contact surface is defined by the Knoop indenter geometry, where a/b = 7.11. Upon unloading, the elastic recovery reduces the length of the shorter dimension, b, to b', while the longer dimension, a, remains relatively uneffected. The recovery depends on the ratio H/E and is independent of load. Marshall et al. have derived the following expression relating b'/a' to H/E :

$$b'/a = b/a - \alpha H/E \qquad (4.1)$$

where α = 0.45. The value of α was determined by fitting Eq.(4.1) to data obtained for a wide range of materials with known H and E.

The optical micrograph of Knoop damage pattern on polished surface of the HAp specimen indented with 5 N load is shown in Fig.4.10. The data of b'/a are plotted as a function of the indentation load P in the load range of 1 to 20 N in Fig.4.11. The data were obtained by an optical microscope. Each data point in Fig.4.11 represents the mean and standard deviation of five indentations. The result illustrated in Fig.4.11 has established that the ratio of impression diagonal, b'/a, in the HAp specimens is independent of indentation load. It can be seen from such plot that the mean value of b'/a = 0.131 $\pm$ 0.004. By using Eq.(4.1) in accordance with H = 5.3 GPa (as evaluated in Sect.4.1.2.1), b/a = 1/7.11 and b'/a = 0.131 $\pm$ 0.004, we obtain E = 274.7 $\pm$ 3.1 GPa.

Having evaluated the values of H (Sect.4.1.2.2.1), E (Sect.4.2), and $P/c^{3/2}$ (Sect.4.1.2.2.2) for HAp specimens, we are now in a position to to evaluate fracture toughness, using Eq. (3.22). Vickers indenter, Antis et al (53) established a vaiue, ξ = 0.016, by calibrating indentation parameters with fracture toughness by conventional fracture mechanics techques. Using Anstis et al. calibtion value of ξ along with E = 274.7 $\pm$ 3.1 GPa. H = 5.3 $\pm$ 0.4 GPa and the mean value of $P/c^{3/2}$ = 8.1 $\pm$ 0.1 $MPam^{-1/2}$ yields T = 0.9 $\pm$0.1 $MPam^{-1/2}$ for HAp specimens.

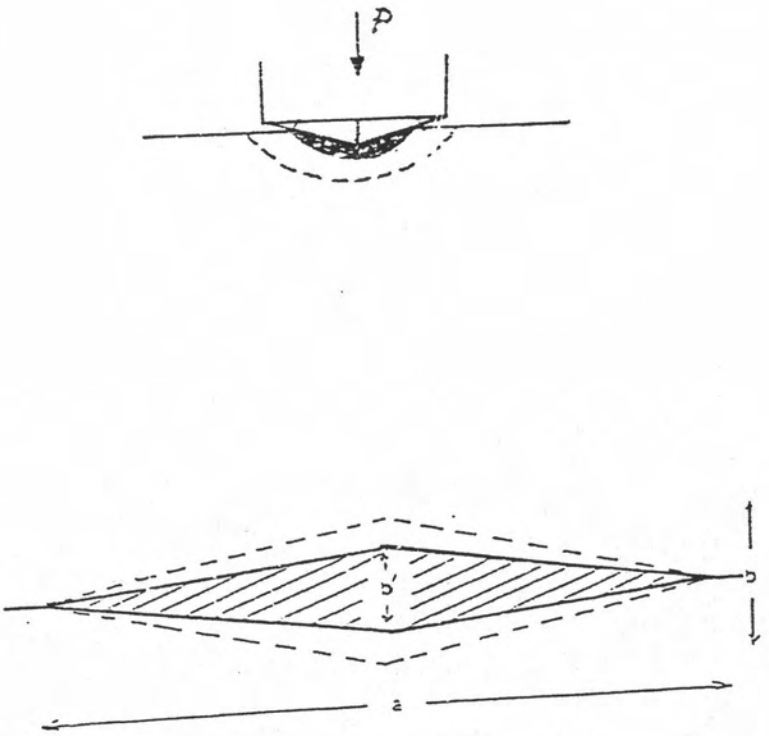

Fig.4.9 Schematic diagrams of Knoop damage. Dash line in the bottom diagram is impression on surface at fuliy loaded state and solid line is impression on surface at unloaded state.

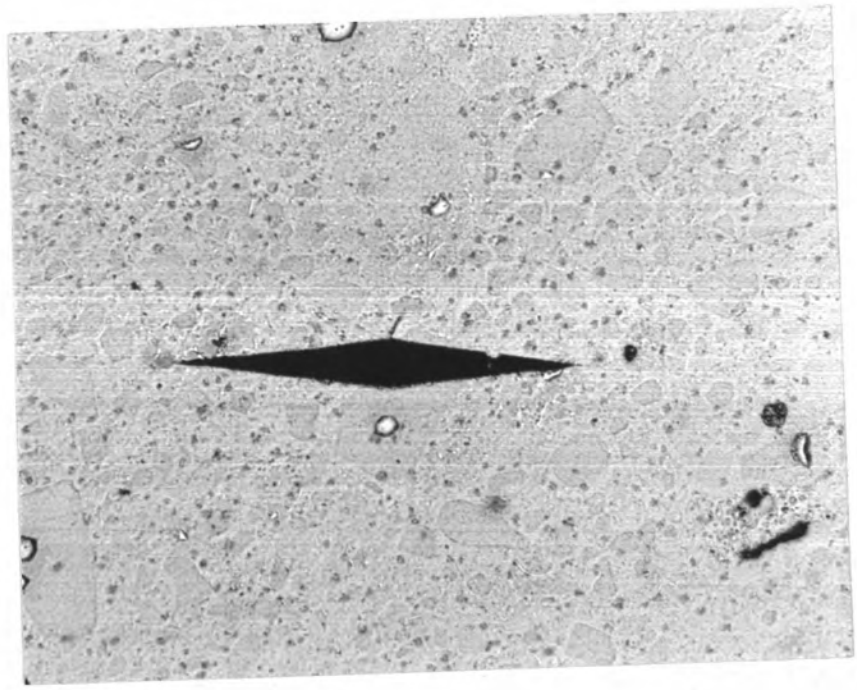

Fig.4.10 Optical micrograph of Knoop impression on surface of the HAp specimen

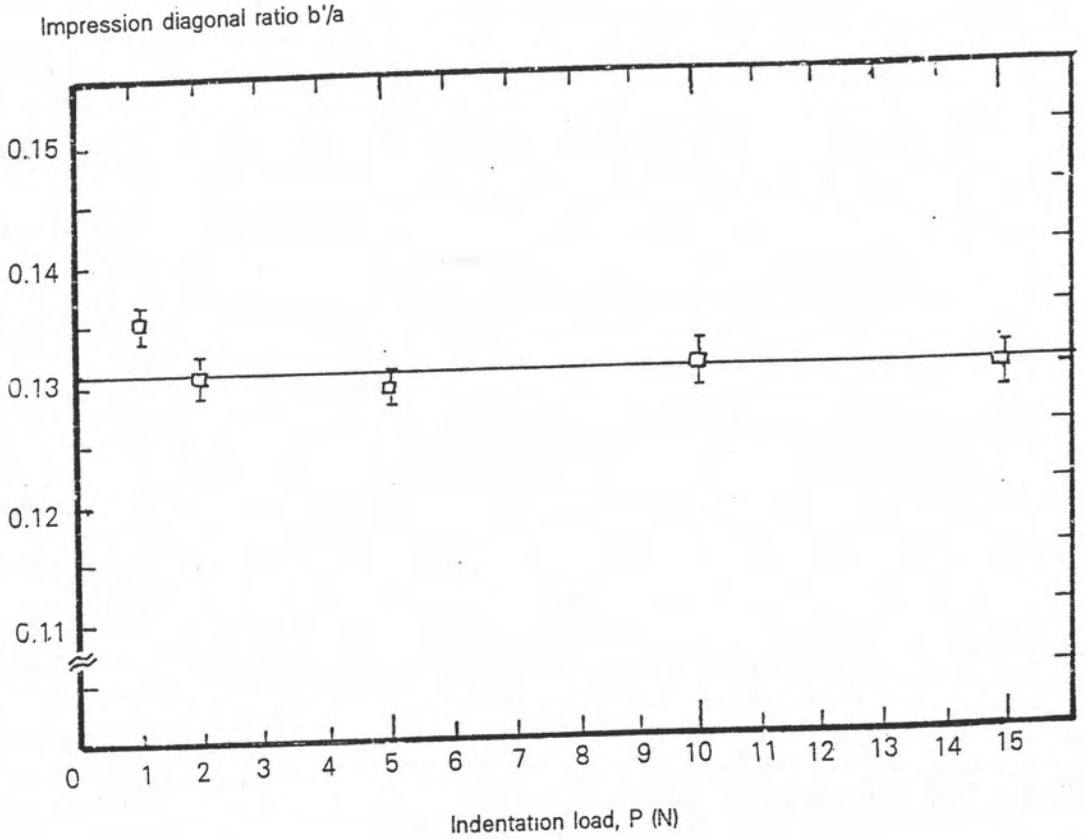

Fig.4.11 Plot of impression diagonal ratio b'/a as a function of indentation load, P, on HAp specimen.

4.3 Indentation-Controlled Strength Test

4.3.1 Experimental Procedure

The jig used for the strength testing in this work was designed and constructed suitable for our HAp specimen shape and dimension. Fig. 4.12 shows the photograph of constituents of the constructed jigs : (i) truncated steel ball, (ii) holder of the truncated steel ball, (iii) three steel ball and (iv) steel block where the three steel balls sit. The experimental setup for this jig is shown in Figs. 4.13 and 4.14. The truncated steel ball (circular flat punch) was mounted into the underside of the crosshead of a universal testing maching (LLOYD) which is attached to a compression load cell (maximum load 2.5 kN). The steel block with the three loading balls was seated on a fixed bar. The indented specimen was mounted on the three loading ball, with the indented face on the tension side. The jig was operated to produce positive concentric alignment of the upper punch and lower three points. This arrangement has been shown to minimise the loading errors due to the effects of specimen warpage (54).

Stresses were calculated from the outer fibre stress of an elastically loaded plate using

$$\sigma = kF/d^2 \qquad (4.2)$$

where F is the applied force, d the specimen thickness and k a constant :

$$k = [\,3/4\,\pi\,][\,\nu(1+2)\ln(a/r_o) + (1-\nu)(2a^2-r_o^2)/2b^2 + (1+\nu)\,] \qquad (4.3)$$

for biaxial loading,where r_o (radius of the upper punch) and a (radius of the lower ring) are the inner and outer semi-spans of the jig, b is the specimen radius and ν is the Poisson's ratio (55). The radius r_o of the flat punch in the biaxial tests was 1.98 mm and the radius a of the outer circle upon which the three loading balls sat was 8.90 mm.

Strength tests were run for the prepared HAp specimens. Each specimen surface was polished with a series of SiC papers (800, 1200 mesh), and alumina powder in water slurry (1 μm). When the polishing process was completed, each specimen was indented at its face center with a Vickers indenter at a prescribed peak load using a hardness tester (Sect.4.1.1).

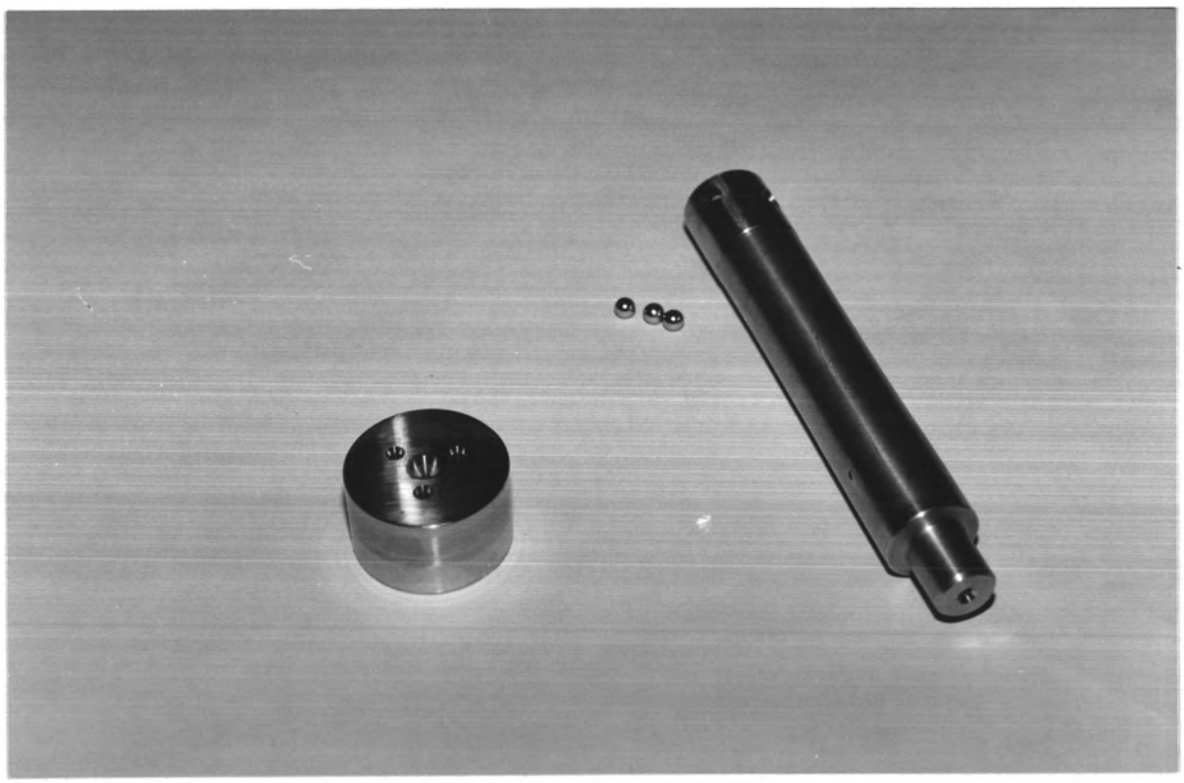

Fig.4.12 Photograph of constituents of the constructed jig:

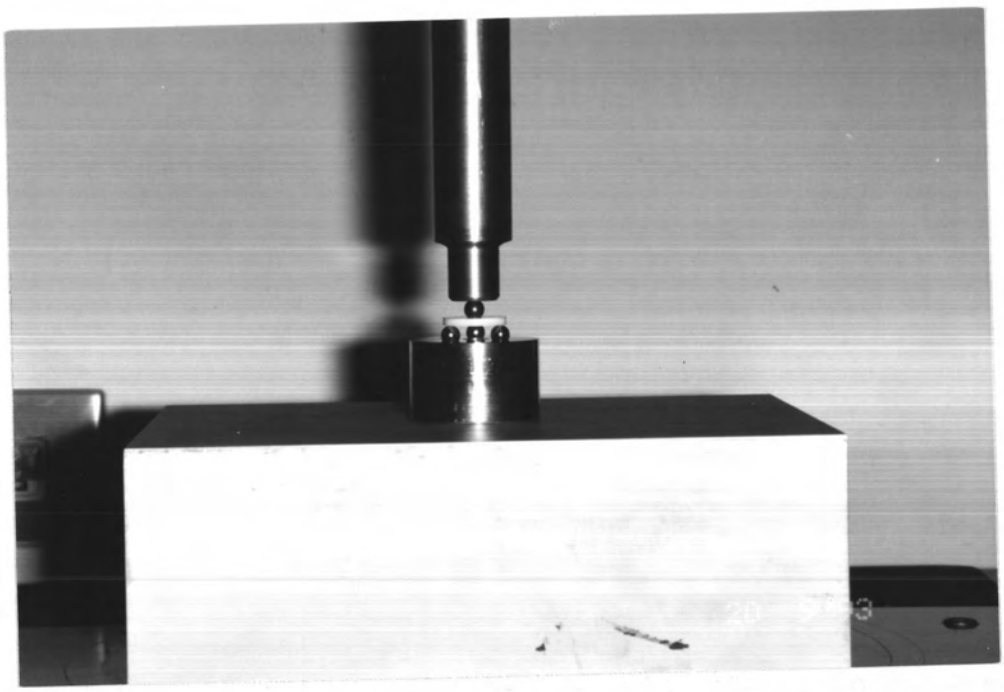

Fig.4.13 Photograph of the flat on three ball apparatus used for the biaxial strength tests.

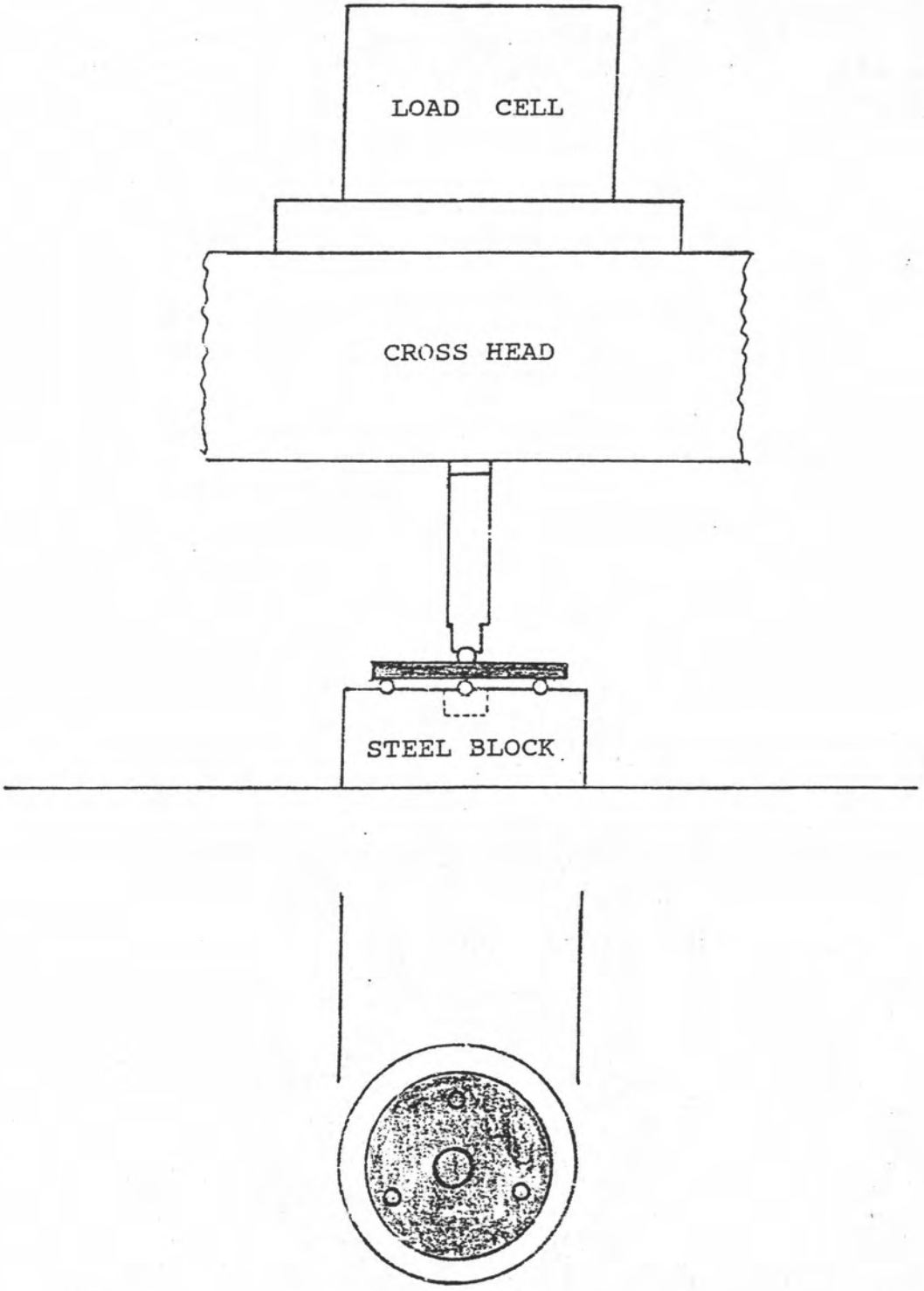

Fig.4.14 Diagram of the flat on three ball apparatus used for the biaxial strength tests. Specimen shown shaded.

Some specimens were left unindented as controls. A drop of silicone oil was placed on the indentation site and the specimen wrapped in polythene tape. The polythene tape used to cover the specimens for testing filled three functions; (i) it kept the testing environment (oil) at the failure site, (ii) it held the specimen pieces together after failure and (iii) it smoothed any asperities at the points of contact between the jig and specimens (minimising stress concentrations at the loading points). The indented specimens were taken to failure in the biaxial test using the crosshead speed of 2 mm min^{-1} to produce failure. The verage interval between indentation and biaxial test was about 3 h, during such time the indentation cracks were exposed to air to allow for saturation of postindentation slow crack growth. All broken specimens were examined optically to confirm that failure had occurred from the indentation site; only a few specimens indented at relatively low indention loads where pre-existing flaws dominate was broken from the other origins. These breaks that did not pass through the indentions were incorporated into the data pool for unindented specimens. Eq. (4.4) was used to evaluate the corresponding tensile stress on the crack.

Scanning electron microscopy was used to examine the fracture surfaces to determine the relative amounts of intergranular and transgranular cracking.

4.3.2 Results

All specimens indented in the load range 10 to 100 N broke from the ndentation sites. The observed strengths are plotted as a function of indentation load in Fig.4.15. Each data point represents the mean and standard deviation of five specimens breaking from the indentation sites at a prescribed load. The shaded band at left represents the strength of non-indented specimens. The inclined solid line through the data point is a least-squares fit to the mean value of quantity of $\sigma P^{-1/3}$ computed over all specimens broken from the indentation crack.

It is found from careful examinations by optical and scanning electron microscopy that the indentation crack path is still purely intragranular after biaxial testing. Fig.4.16 is an example of indentation crack path after biaxial testing. Grain-interlocked bridgings at crack interfaces cannot be found in the HAp specimens.

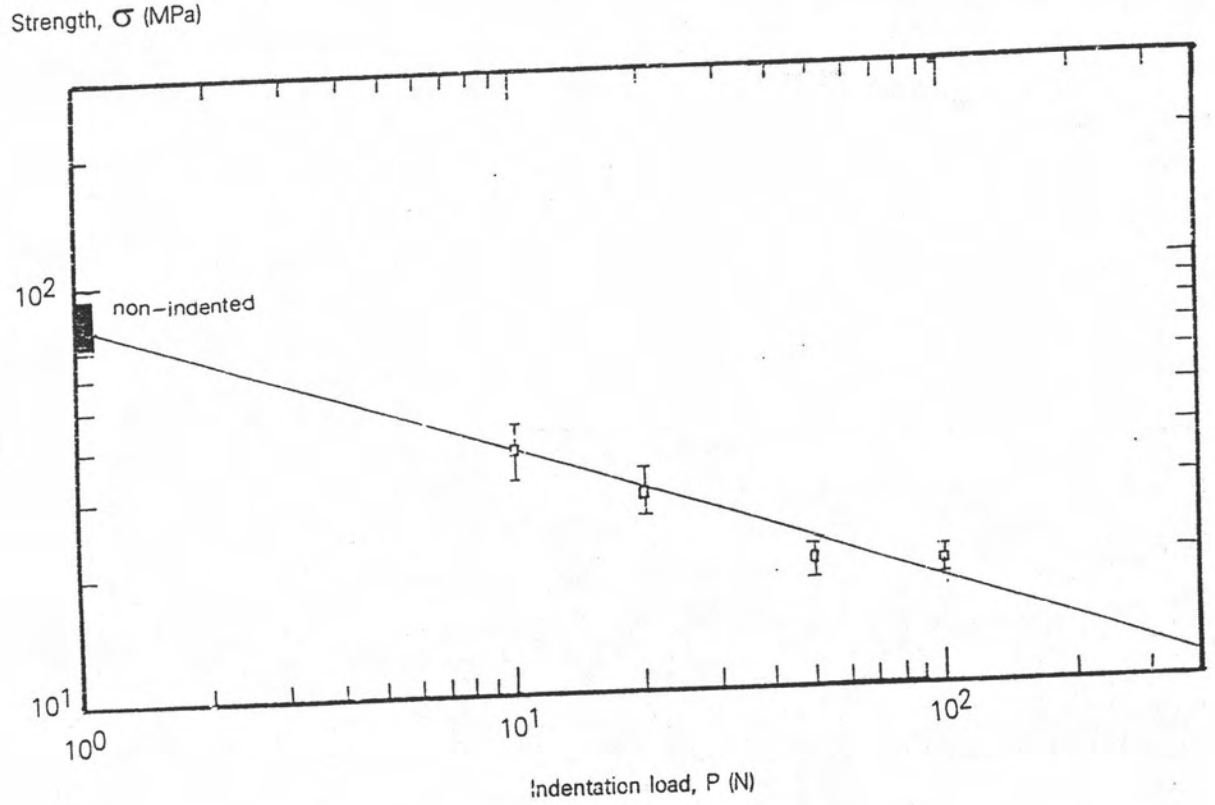

Fig.4.15 Plot of strength as a function of indentation load,P.

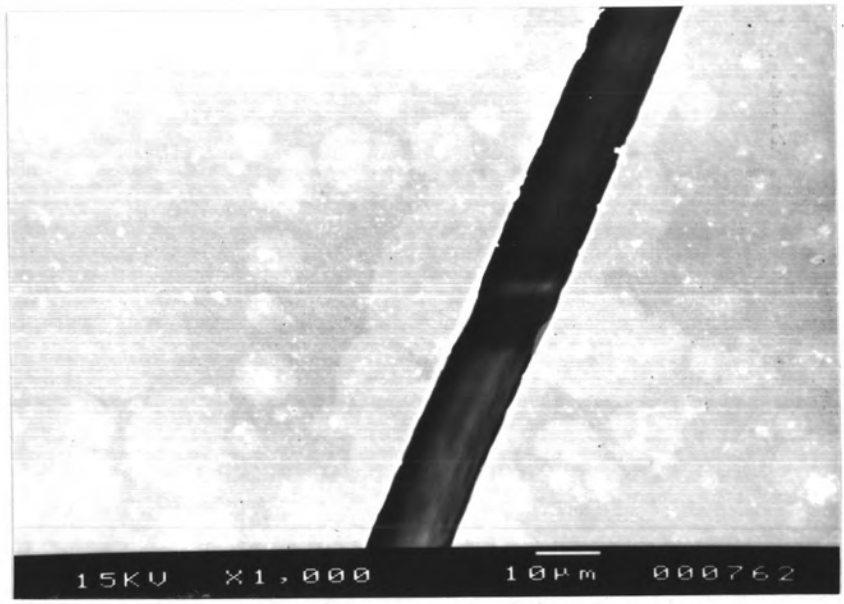

Fig.4.16 SEM micrograph showing the indentation crack path in HAp specimen which broke from the indentation crack.

4.4 Discussion and Conclusion

The damage pattern produced on HAp surfaces by a Vickers indenter is studied. It is found to consist of a square impression and two crack systems, i.e. the median/radial crack and lateral crack (Figs.4.1-4.3). Although such damage patterns are artificially produced, there is a considerable evidence that it has the essential qualities of naturally occurring cracks which have contact history(49): cracks introduced by scratching, surface finishing process and spurious particle contact are just a few pertinent examples. It is found in this work that a relatively large median/radial crack, which is the likely source of premature failure, can be easily formed even at the indentation load as low as 1 N (Fig.4.1). The intersection of lateral crack to specimen surface, which causes surface chipping,is observed even at this low indentation load. Thus these observations indicate that HAp specimens fabricated in this work (Chap.2) are highly susceptible to microcrack formations due to handling damages, thus resulting in both strength degradations and surface removals of HAp ceramics.

From the direct measurement of the impression diagonals and the median/radial crack lengths from damage patterns due to Vickers and Knoop indentations as a function of indentation load (Figs.4.5-4.8, 4.11), the following average mechanical properties of HAp specimens are found : hardness H, 5.3 $\pm$ 0.4 GPa; stiffness E, 274.4 $\pm$ 3.1 GPa; and fracture toughness T,0.9 $\pm$ 0.1 $MPam^{1/2}$

The results of the indentation-strength tests are summarized in Fig.4.15. A reasonably agreement between the data points and the inclined solid line illustrates that strengths of the HAp ceramics tend to follow the -1/3 power law dependence of strength on indentation load. As being shown in Sect.3.4 that this law (Eq.(3.30)) is based on the presumption of a single-value fracture toughness, therefore the indentation-strength results indicate that HAp ceramics has a single-value fracture toughness and its strength is strongly dependent on the pre-existent crack size. The physical insight into the conclusion that the HAp ceramics has a single - value toughness is available from the results obtained from optical and SEM examinations that its cracks always propagate through the grains (Figs. 4.4 and 4.16) and no grain-interlocked

bridgings are found at crack interfaces. Thus the toughening mechanisms of grain-interlocked bridgings, which can dissipate energy from the loading system and results in the increase in fracture toughness as the crack length increases (T-curve) as described in Sect.3.5.1, are not possible in the HAp ceramics. These results indicate that the grain boundary toughness of HAp ceramics has a higher value than its average fracture toughness, therefore cracks tend to propagate through the grains (intragranular) rather than along the grain boundaries (intergranular) . Accordingly, eventhough the HAp ceramics should have lock-in thermal expansion mismatch stresses due to its noncubic structure as in many monophase ceramics displaying the T-curve, the grains cannot be clamped by these lock-in stresses since cracks do not propagate along the grain boundary. Therefore for the next part of this work, we will not make an attempt to modify its microstructure by changing its grain sizes and shapes, but we will disperse Y_2O_3-ZrO_2 uniformiy into the HAp matrix to promote phase-transformation toughening.